Superlattices and Microstructures 142 (2020) 106519

Contents lists available at ScienceDirect

Superlattices and Microstructures

journal homepage: www.elsevier.com/locate/yspmi

Theoretical prediction of electronic and optical properties of haft-hydrogenated InN monolayers

Dat D. Vo [a,b], Tuan V. Vu [a,b], Le C. Nhan [c], Chuong V. Nguyen [d], Huynh V. Phuc [e], Hien D. Tong [f], D.M. Hoat [g], Le T. Hoa [h,i,*], Nguyen N. Hieu [h,i]

[a] Division of Computational Physics, Institute for Computational Science, Ton Duc Thang University, Ho Chi Minh City, Viet Nam
[b] Faculty of Electrical & Electronics Engineering, Ton Duc Thang University, Ho Chi Minh City, Viet Nam
[c] Department of Environmental Science, Sai Gon University, Ho Chi Minh City, Viet Nam
[d] Department of Materials Science & Engineering, Le Quy Don Technical University, Ha Noi, Viet Nam
[e] Division of Theoretical Physics, Dong Thap University, Cao Lanh, Viet Nam
[f] Faculty of Engineering, Vietnamese–German University, Binh Duong, Viet Nam
[g] Computational Laboratory for Advanced Materials and Structures, Advanced Institute of Materials Science, Ton Duc Thang University, Ho Chi Minh City, Viet Nam
[h] Institute of Research and Development, Duy Tan University, Da Nang 550000, Viet Nam
[i] Faculty of Natural Sciences, Duy Tan University, Da Nang 550000, Viet Nam

ARTICLE INFO

Keywords:
Monolayer InN
Haft-hydrogenation
Electronic states
Optical characteristics
First-principles calculations

ABSTRACT

In this work, we investigate the electronic and optical properties of two configurations of haft-hydrogenated indium nitride monolayers H–InN and 2H–InN using first-principles calculations. Both H–InN and 2H–InN monolayers are semiconductors with indirect bandgap quite larger than that of pure InN monolayer. When the spin–orbit coupling was included, their bandgap is significantly reduced. Upon the hydrogenation, charge transfers from InN plane to functionalized species H in H–InN while a small amount of charge has been transferred from H atoms to InN plane in 2H–InN monolayer. Haft-hydrogenated InN monolayers can strongly absorb light in a wide range from visible light to infrared which opens possibilities for their application in optoelectronic devices.

1. Introduction

Since its discovery in 2004, graphene has been a hot material of interest to scientists for more than 15 years because of its outstanding physical and chemical properties [1]. The success of the application of graphene in nanoelectronic devices has spurred a large-scale search of two-dimensional (2D) layered materials [2–8]. A series of 2D graphene-like structures, such as silicene, germanene, transition metal dichalcogenides or monochalcogenides, were discovered and studied extensively [9–12]. Recently, Şahin and co-workers have shown that the group III–V binary compounds have many extraordinary properties [13], which do not exist in other 2D hexagonal structures, with potential applications in optoelectronic and photocatalytic devices [14,15]. Nitride-based compounds have also attracted a lot of interest because they have many interesting physical properties [16–18].

Monolayer InN is group III–V binary compound formed from In and N atoms. Unlike another group III–V binary compounds containing In, such as InP, InAs and InSb, monolayer InN has a planar structure (all InP, InAs, and InSb monolayers have low-bucking structures) [13]. At equilibrium, calculated energy gap of bulk InN using Heyd–Scuseria–Ernzerhof hybrid functional

* Corresponding author at: Institute of Research and Development, Duy Tan University, Da Nang 550000, Viet Nam.
E-mail addresses: voduydat@tdtu.edu.vn (D.D. Vo), vuvantuan@tdtu.edu.vn (T.V. Vu), hvphuc@dthu.edu.vn (H.V. Phuc), lethihoa8@duytan.edu.vn (L.T. Hoa).

https://doi.org/10.1016/j.spmi.2020.106519
Received 7 February 2020; Received in revised form 4 April 2020; Accepted 9 April 2020
Available online 13 April 2020

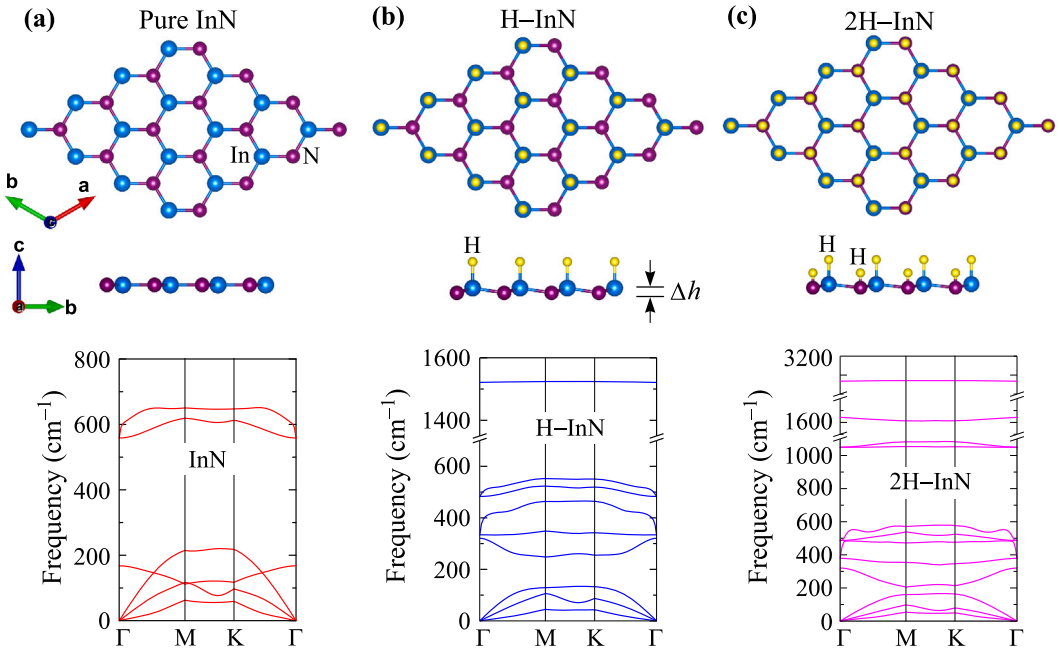

Fig. 1. Different views of optimized atomic structure (top panel) and phonon spectra (bottom panel) of (a) pure InN, (b) H–InN, and (c) 2H–InN monolayers.

is 0.50 eV [19]. Monolayer InN is a semiconductor with a small energy gap around 0.6 eV [13,16]. Monolayer InN has been experimentally synthesized by different methods with band gap varying from 0.63 eV to 0.72 eV [20–22]. Previous studies have shown that similar to other two-dimensional (2D) monolayers, electronic properties of monolayer InN are also very sensitive to external influences such as strain engineering [23] or defects [24]. Also, monolayer InN has thermal stability up to 600 K and can sustain under large strain engineering [25]. In addition to traditional methods of changing physical properties of materials such as strain engineering [26], electric fields [27] and forming heterostructures [28–32] or place on the semiconductor substrates, a new way has been proposed and proved effective for controlling the physical and chemical properties of 2D monolayers being the chemically functionalization their surface with atomic gases [33]. Recent studies have demonstrated that surface functionalization of 2D layered materials can lead to the emergence of new properties that do not exist in pure materials [34–36]. Hydrogenation of bulk InN has been experimentally studied for a long time [37]. Fu and co-workers have shown that hydrogenation enhances the peak intensity of the photoluminescence spectra in the InN epifilms [38]. The change in physical properties, especially the opto-electronic properties, of the 2D layered materials in general and monolayer InN in particular when their surfaces are functionalized opening possibilities for their application in the next-generation devices.

In the present work, we systematically consider the electronic and optical properties of two kinds of haft-hydrogenated InN monolayers i.e, the H–InN and 2H–InN monolayers, using the density functional theory. We focus on investigating the changes in geometric structure, band structure and optical characteristics of a monolayer InN when it was haft-functionalized with hydrogen atoms.

2. Methodology

All simulations in this Letter were performed based on density functional theory (DFT) using the Quantum Espresso code [39]. We use the generalized gradient approximation (GGA) suggested by Perdew–Burke–Ernzerhof (PBE) [40,41] as exchange–correlation potential. The spin–orbit coupling (SOC) was included in all self-consistent simulations for electronic structures [42]. The projector augmented wave method is used to consider the electronic properties of monolayers. The norm conserving pseudopotential [43] was used and the cut-off of energy for a plane-wave basis is set to be 500 eV. In our calculations, we use a $(15 \times 15 \times 1)$ k-mesh in the Brillouin zone. To optimize the structures of the monolayers, the criteria for energy and force convergence was used in our calculations being 10^{-6} eV and 10^{-3} eV/Å, respectively. Also, it is well-known that the PBE functional underestimates the band gap of the semiconductors [44]. To correct the band structures and energy gap values, calculations by Heyd–Scuseria–Ernzerhof (HSE06) hybrid functional [45] are carried out. To eliminate the interactions which may exist between neighbor slabs, we use a large vertical vacuum space of 20 Å in our calculations.

Table 1
Calculated lattice constant a, bond lengths d, and buckling constant Δh (Å). Obtained band gaps (in units of eV) by the PBE functional E_g^{PBE}, PBE+SOC method $E_g^{\mathrm{PBE+SOC}}$, and HSE06 hybrid functional E_g^{HSE06} and binding energy E_b (eV).

Configuration	a	$d_{\mathrm{In–N}}$	$d_{\mathrm{In–H}}$	$d_{\mathrm{N–H}}$	Δh	E_g^{PBE}	$E_g^{\mathrm{PBE+SOC}}$	E_g^{HSE06}	E_b
InN	3.616	2.088	–	–	0	0.710	0.237	1.721	−12.126
H–InN	3.647	2.13	1.757	–	0.320	2.260	1.815	3.157	−13.660
2H–InN	3.848	2.236	1.722	1.045	0.249	2.648	2.332	3.594	−18.673

3. Results and discussion

Atomic structures after fully relaxation of pure InN and haft-hydrogenated InN monolayers are shown in Fig. 1. In this work, we consider two configurations of haft-hydrogenated InN monolayer (or one-side hydrogenated InN monolayer). There are one hydrogen atom bonded directly with the In atoms H–InN monolayer [Fig. 1(c)] and two hydrogen atoms bonded with the In and N atoms on the same side 2H–InN [Fig. 1(c)]. Our calculations demonstrate that after fully relaxation, while the pure InN monolayer has a planar structure, both two configurations of haft-hydrogenated InN monolayers have a low-bucking structure and the bucking constant Δh for the H–InN and 2H–InN monolayer is 0.320 Å and 0.249 Å, respectively. After fully relaxation, the lattice constant of the pure InN monolayer is 3.616 Å. Our obtained result for lattice constant of the pure InN monolayer is close to the calculated result of Zhuang and co-workers (3.63 Å) [46]. Compared to pure InN monolayer, haft-hydrogenation has increased the lattice constant of the system, particularly in the case of 2H–InN monolayer (3.848 Å). Besides, the difference in bonding lengths between hydrogen and In $d_{\mathrm{In–H}}$ and N $d_{\mathrm{N–H}}$ atoms in the 2H–InN monolayer is quite large. These bond lengths are $d_{\mathrm{In–H}} = 1.722$ Å and N $d_{\mathrm{N–H}} = 1.045$ Å. We listed the lattice parameters of both pure InN and haft-hydrogenated InN monolayer in Table 1. To check the dynamical stability, the phonon spectra of pure InN, H–InN and 2H–InN monolayers have been calculated. As shown in the bottom panel of Fig. 1, we can see that no soft modes (imaginary frequencies) are found in the phonon dispersion curves, guaranteeing that the monolayers are dynamical stable.

The binding energy E_b of the monolayers is calculated by the follows

$$E_b = E_{\mathrm{tot}} - n_{\mathrm{In}}E_{\mathrm{In}} - n_{\mathrm{N}}E_{\mathrm{N}} - n_{\mathrm{H}}E_{\mathrm{H}}, \tag{1}$$

where E_{tot} is the total energy of the InN monolayer, E_{X} and n_{X} are the total energy of the X atom (X = In, N, H) and numbers of the X atoms in the simulated cells, respectively. Our calculated results reveals that the binding energy of all configurations InN, H–InN, and 2H–InN is negative. The binding energy E_b for the InN, H–InN, and 2H–InN monolayers is $E_b^{\mathrm{InN}} = -12.126$ eV, $E_b^{\mathrm{H–InN}} = -13.660$ eV, and $E_b^{\mathrm{2H–InN}} = -18.673$ eV, respectively. The negative binding energy calculated by Eq. (1) implied that the binding between atoms is strong in the monolayer InN and haft-hydrogenated InN monolayers. In case the InN monolayer is hydrogenated with one hydrogen atom as shown in Fig. 1(a), in principle, there are two possible configurations: H–InN and InN–H. Our calculations have shown that H–InN configuration is most stable configuration. Therefore, in this work we only investigate this configuration.

Band structures of pure InN and haft-hydrogenated InN monolayers are depicted in Fig. 2. Our DFT simulations demonstrate that both pure InN and haft-hydrogenated InN monolayers are indirect semiconductors. The band gap of pure InN monolayer at equilibrium is 0.710 eV at the PBE level. This result is close to the available experimental data (around 0.7 eV) [20–22]. Upon haft-hydrogenation, the band gap of hydrogenated InN monolayers increases significantly to 2.260 eV for the H–InN monolayer and 2.648 eV for the 2H–InN monolayer. Focusing on the contributions of atomic orbitals to the forming of the electronic bands of the monolayers, we also plotted the partial density of states (PDOS) of monolayers as shown in Fig. 2. We can see that, in two configurations of hydrogenated InN monolayers, the contributions of the orbitals of the N atoms are larger than that of the In atoms in the valence bands. However, the contribution of the orbitals of the In to the conduction band is more prominent than that of the N atoms. Besides, the contribution of the $\mathrm{H_{In}}$-s orbital ($\mathrm{H_{In}}$ refers to the H atom that is directly bonded to the N atom in the monolayers) to electronic bands is superior to that of the $\mathrm{H_N}$-s orbital.

It is well-known that the PBE functional underestimates the band gap of the semiconductors [44]. One also showed that Heyd–Scuseria–Ernzerhof (HSE06) hybrid functional [45] or the GW approximation [47] can be estimated more accuracy the energy gap of semiconductors. Therefore, in this work, along with the PBE functional, the HSE06 functional [45] was used to calculate the band gap of the monolayers. As shown in Fig. 2, we can see that the calculated band structures of monolayers using the HSE06 and PBE functionals have the same profile. Calculated band gaps of the InN, H–InN, and 2H–InN monolayers are also listed in Table 1. We can see that the calculated results for band gaps by the HSE give much larger value than that by the PBE method.

We already know that influences of the spin–orbit coupling (SOC) on the electronic states of 2D monolayers are quite important. When the SOC is included, the band structure of the monolayers, especially the valence band, is significantly changed. In Fig. 3(a), we show the band structures of pure InN and haft-hydrogenated InN monolayers calculated by the PBE+SOC method. Our obtained results indicate that when the SOC is included, small orbit-splitting energy has appeared in the valence band. Also, the PBE+SOC method has shown that the energy gap of InN monolayers has decreased significantly when the SOC is included. Calculated band gaps of the pure InN and haft-hydrogenated InN monolayers by both the PBE and PBE+SOC methods are depicted in Fig. 3(b). From Fig. 3(b) we can see that although the SOC effect reduces the band gap of monolayers, this reduction is uneven. While the SOC effect reduces up to 67% of the band gap of the pure InN monolayer (reduced from 0.710 eV to 0.237 eV), the band gap of the haft-hydrogenated InN monolayer is only reduced by 20% for the H–InN monolayer or 12% for the 2H–InN monolayer when the SOC is included.

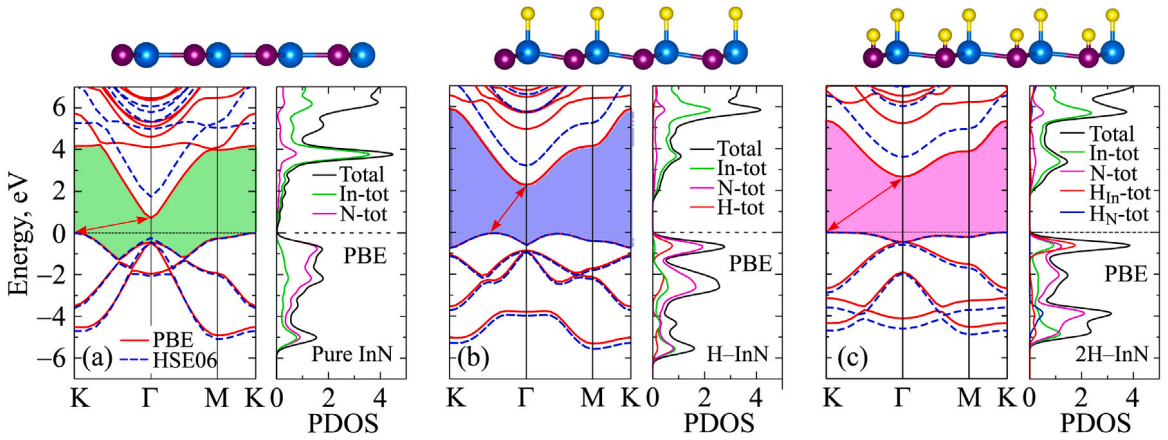

Fig. 2. Calculated band structures and PDOS of the pure InN (a), haft-hydrogenated N–InN (b) and 2H–InN (c) monolayers using the PBE functional.

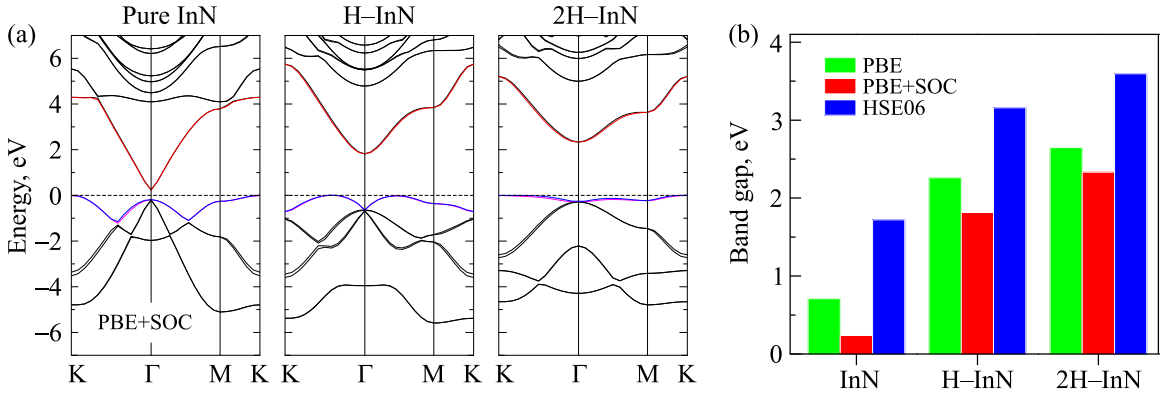

Fig. 3. (a) Calculated band structures of haft-hydrogenated InN monolayers using PBD+SOC approach and (b) band gap of haft-hydrogenated InN monolayers.

Table 2
Internal charge of constituent atoms and transferred charge between InN plane and functionalizated species H (in unit of *e*) in pure InN and haft-hydrogenated InN monolayers.

Configuration		*s*	*p*	Total	Charge	Transferred charge
InN	In	0.85	1.0	1.85	1.15	–
	N	1.75	4.4	6.15	−1.15	
H–InN	H	1.19	–	1.19	−0.19	+0.19
	In	0.79	1.07	1.86	1.14	
	N	1.80	4.15	5.95	−0.95	
2H–InN	H_{In}	1.28	–	1.28	−0.28	−0.03
	H_N	0.70	–	0.70	0.30	
	In	0.90	1.05	1.96	1.04	
	N	1.77	4.30	6.07	−1.07	

Together with the calculations for the PDOS, where we can see the contribution of atom orbitals to the formation of electronic bands, we performed calculations for the electron density to see the distribution of electrons in atoms of the systems. Contour plot of the electron density of atoms in the pure InN monolayer and two configurations of haft-hydrogenated InN monolayers is shown in Fig. 4. Fig. 4 reveals that the electron density is enriched in both N and In atoms. In the cases of hydrogenated InN monolayers, electron enrichment is just for the H_N atoms as shown in Fig. 4(c). The distribution of electronic charger in the H_{In} atoms in both cases of H–InN [Fig. 4(b)] and 2H–InN [Fig. 4(c)] is small. Also, we perform the calculations for the internal distribution of charge and transferred charge between atoms in the haft-hydrogenated InN monolayers using the Mulliken population analysis [48]. The calculated internal charge distribution of constituent atoms in the pure InN and haft-hydrogenated InN monolayers using the Mulliken population analysis is listed in Table 2. Our calculated results reveal that while the charge transfers from the InN monolayer to functionalized species H in the H–InN configuration, a small amount of charge has been transferred from H species to the InN monolayer in the 2H–InN monolayer when the InN monolayer is haft-functionalized by the hydrogen atoms.

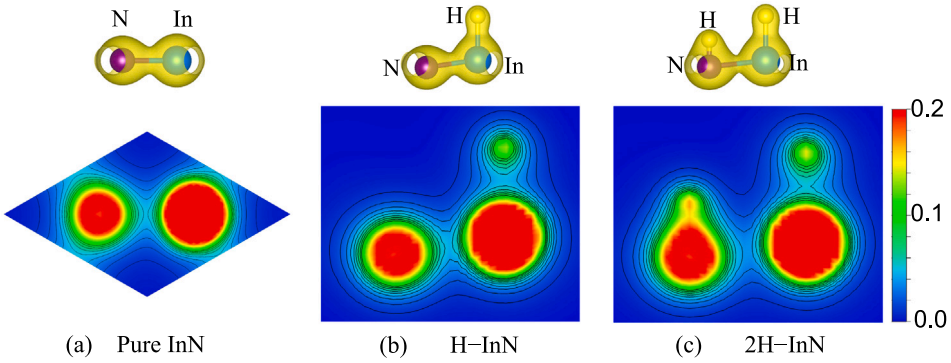

Fig. 4. Contour plot of electron density of atoms with 0.02 Bohr^3 interval from 0 to 0.2 e/Bohr^{-3} of the pure InN (a), H–InN (b), and 2H–InN (c) monolayers.

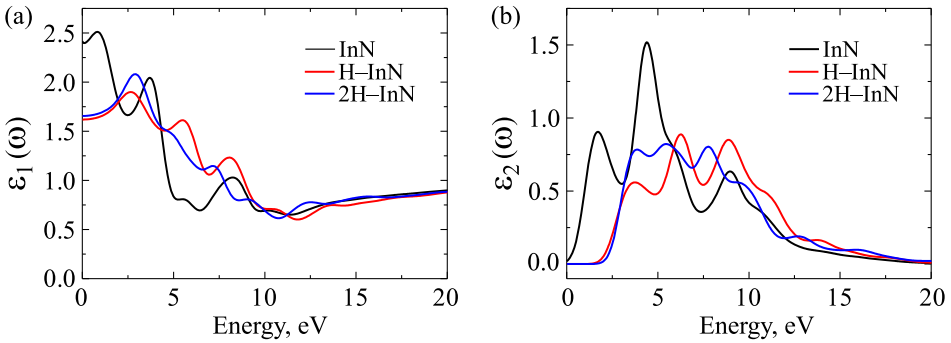

Fig. 5. Dielectric function of pure InN monolayer and haft-hydrogenated H–InN and 2H–InN monolayers: (a) real part $\varepsilon_1(\omega)$ and (b) imaginary part $\varepsilon_2(\omega)$.

In this part, we examine the optical characteristics of the two configurations H–InN and 2H–InN. The dielectric function $\varepsilon(\omega) = \varepsilon_1(\omega)+i\varepsilon_2(\omega)$ and the absorption coefficient $A(\omega)$ of these haft-hydrogenated InN monolayers will be focused investigation. The incoming parallel polarized light (along the a-axis) with photon energy in the interval from 0 to 20 eV was used in this calculation.

Actually, the imaginary part $\varepsilon_2(\omega)$ can be estimated first by sum of the occupied–unoccupied transitions and the real part $\varepsilon_1(\omega)$ can be obtained via the Kramer–Kronig transformation. The parts of the dielectric function $\varepsilon_2(\omega)$ and $\varepsilon_2(\omega)$ can be expressed as the following [49,50]

$$\varepsilon_2^{ij}(\omega) = \frac{Ve^2}{2\pi\hbar m^2\omega^2}\int d^3\mathbf{k}\sum_{nn'}\langle \mathbf{k}n\left|p_i\right|\mathbf{k}n'\rangle\langle \mathbf{k}n'\left|p_j\right|\mathbf{k}n\rangle \times f_{\mathbf{k}n}(1-f_{\mathbf{k}n'})\delta(E_{\mathbf{k}n'}-E_{\mathbf{k}n}-\hbar\omega), \tag{2}$$

and

$$\varepsilon_1(\omega) = 1+\frac{2}{\pi}P\int_0^\infty \frac{\omega'\varepsilon_2(\omega')}{\omega'^2-\omega^2}d\omega', \tag{3}$$

where ω is the frequency of the incoming electromagnetic irradiation, $|\mathbf{k}n\rangle$ part stands for the crystal wave-function regarding to energy $E_{\mathbf{k}n}$ with $\mathbf{k}$ being the wavevector, $\mathbf{p} = (p_x, p_y, p_z)$ is the momentum operator, $f_{\mathbf{k}n}$ is the function of the Fermi distribution, V is the volume of the unit cell, and P stands for the principal value of the integral.

In Fig. 5, we present the calculated results for the dielectric function of the haft-hydrogenated InN monolayers under incoming light perpendicularly polarized in the energy domain from 0 to 20 eV. Also, the parts of the $\varepsilon(\omega)$ of the pure InN monolayer are calculated for comparison. Our calculated results reveal that the imaginary part $\varepsilon_2(\omega)$ of the dielectric function of both H–InN and 2H–InN monolayers does not a response to the parallel polarized light in the low energy domain from 0 to 2 eV. Compared to the pure InN monolayer, where the first optical gap is in the visible light region, the first optical gaps of the haft-hydrogenated InN monolayers are in the ultraviolet region. As shown in Fig. 5(b), the first optical gaps in the H–InN and 2H–InN monolayers are in 3.748 eV and 3.859 eV, respectively. It means that the first optical gap of the pure InN monolayer (at 1.706 eV) has shifted quite a bit from the visible light region to the ultraviolet region upon the functionalization with hydrogen atoms.

The absorption coefficient $A(\omega)$ and optical reflectivity $R(\omega)$ can be defined via the $\varepsilon(\omega)$ function which is given by [50,51]

$$A(\omega) = \frac{\sqrt{2}\omega}{c}\left[\sqrt{\varepsilon_1^2(\omega)+\varepsilon_2^2(\omega)}-\varepsilon_1(\omega)\right]^{1/2}, \tag{4}$$

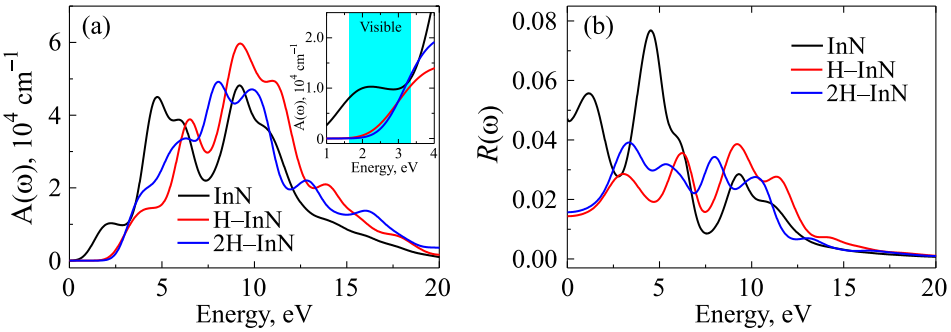

Fig. 6. Absorption coefficient $A(\omega)$ (a) and optical reflectivity (b) of pure InN monolayer and haft-hydrogenated H–InN and 2H–InN monolayers.

$$R^{ij}(\omega) = \left| \frac{\sqrt{\varepsilon_1^{ij} + i\varepsilon_2^{ij}} - 1}{\sqrt{\varepsilon_1^{ij} + i\varepsilon_2^{ij}} + 1} \right|^2 . \tag{5}$$

The calculated absorption coefficient $A(\omega)$ and optical reflectivity $R(\omega)$ of the pure InN monolayer and haft-hydrogenated indium nitride H–InN and 2H–InN monolayers are shown in Fig. 6(a) and (b), respectively. As depicted in Fig. 6(a), we can see that the whole the $A(\omega)$ of pure InN monolayer absorbs strongly the visible light, the haft-hydrogenated InN monolayers (both two configurations H–InN and 2H–InN) absorb strongly the light in the ultraviolet region. Upon the haft-hydrogenation, the $A(\omega)$ of the H–InN and 2H–InN monolayers changes significantly. The absorption coefficient of both H–InN and 2H–InN monolayer is quite high in the ultraviolet region. Compared to other configurations, the H–InN monolayer has the highest absorption coefficient. The maximum absorption coefficient for the H–InN monolayer is up to 5.970×10^4 cm^{-1} at the incoming photon energy of 9.230 eV compared with 4.918×10^4 cm^{-1} at 8.049 eV in the case of the 2H–InN monolayer and 4.818×10^4 cm^{-1} at 9.206 eV for the pure InN monolayer. Focusing on the visible region as depicted in the inset in Fig. 6(a), we can see that the pure InN monolayer strongly absorbs the visible light with an optical peak located at 2.248 eV while the absorption coefficient of the haft-hydrogenated InN monolayers increases sharply in the visible light region. In the visible light region, the absorption coefficient of the 2H–InN monolayer reaches to 1.20×10^4 cm^{-1} at incoming photon energy of 3.3 eV, slightly greater than that of both pure InN monolayer ($A(\omega)_{max}^{\text{InN}} = 1.03 \times 10^4$ cm^{-1} at 2.248 eV) and the H–InN monolayer ($A(\omega)_{max}^{\text{H–InN}} = 1.01 \times 10^4$ cm^{-1} at 3.3 eV) in this region. Fig. 6(b) shows the optical reflectivity $R(\omega)$ of the monolayers in the energy region from 0 to 20 eV. We see that, in a fairly wide energy domain, from 0 to 10 eV, the optical reflectivity of the haft-hydrogenated InN monolayers is only varying around 0.03. In the larger energy domain of the incoming light, the optical reflectivity of both pure InN and haft-hydrogenated InN monolayers are reduced and asymptotic to zero.

4. Conclusion

We have systematically investigated the electronic states and optical characteristics of haft-hydrogenated InN monolayers using first-principles calculations. Our calculations demonstrated that both H–InN and 2H–InN monolayers are indirect semiconductors with band gaps quite higher than that of the pure InN monolayer. While the charge has been transferred from InN monolayer to the H species in the H–InN configuration, a small amount of charge from the H species in the 2H–InN configuration has been transferred to the InN monolayer. Haft-hydrogenation not only changes the electronic structure of the InN monolayer but also changes its optical characteristics significantly. With a wide range of light absorption, especially strong absorption in the ultraviolet light domain, the haft-hydrogenated InN monolayers are expected to have many potential applications in optoelectronic devices.

Declaration of competing interest

The authors declare that they have no known competing financial interests or personal relationships that could have appeared to influence the work reported in this paper.

CRediT authorship contribution statement

Dat D. Vo: Software, Investigation, Validation. **Tuan V. Vu:** Conceptualization, Methodology, Software, Investigation, Writing - original draft. **Le C. Nhan:** Investigation, Software, Validation. **Chuong V. Nguyen:** Conceptualization, Software, Investigation, Validation. **Huynh V. Phuc:** Conceptualization, Software, Investigation, Validation, Writing - original draft, Writing - review & editing. **Hien D. Tong:** Investigation, Software, Validation. **D.M. Hoat:** Methodology, Investigation, Validation. **Le T. Hoa:** Investigation, Validation, Writing - review & editing. **Nguyen N. Hieu:** Conceptualization, Supervision, Writing - original draft, Writing - review & editing.

References

[1] K.S. Novoselov, A.K. Geim, S.V. Morozov, D. Jiang, Y. Zhang, S.V. Dubonos, I.V. Grigorieva, A.A. Firsov, Electric field effect in atomically thin carbon films, Science 306 (2004) 666.
[2] H.T.T. Nguyen, T.V. Vu, N.T.T. Binh, D.M. Hoat, N.V. Hieu, N.T.T. Anh, C.V. Nguyen, H.V. Phuc, H.R. Jappor, M.M. Obeid, N.N. Hieu, Chem. Phys. 529 (2020) 110543.
[3] K.D. Pham, C.V. Nguyen, H.V. Phuc, T.V. Vu, N.V. Hieu, B.D. Hoi, L.C. Nhan, V.Q. Nha, N.N. Hieu, Superlattices Microstruct. 120 (2018) 501.
[4] T.V. Vu, N.V. Hieu, L.T.P. Thao, N.N. Hieu, H.V. Phuc, H.D. Bui, M. Idrees, B. Amin, L.M. Duc, C.V. Nguyen, Phys. Chem. Chem. Phys. 21 (2019) 22140.
[5] T.V. Vu, H.D. Tong, D.P. Tran, N.T.T. Binh, C.V. Nguyen, H.V. Phuc, H.M. Do, N.N. Hieu, RSC Adv. 9 (2019) 41058.
[6] T.V. Vu, N.V. Hieu, H.V. Phuc, N.N. Hieu, H.D. Bui, M. Idrees, B. Amin, C.V. Nguyen, Appl. Surf. Sci. 507 (2020) 145036.
[7] D.Q. Khoa, C.V. Nguyen, H.V. Phuc, V.V. Ilyasov, T.V. Vu, N.Q. Cuong, B.D. Hoi, D.V. Lu, E. Feddi, M. El-Yadri, M. Farkous, N.N. Hieu, Physica B: Condens. Matter. 545 (2018) 255.
[8] T.V. Vu, A.A. Lavrentyev, D.V. Thuan, C.V. Nguyen, O.Y. Khyzhun, B.V. Gabrelian, K.C. Tran, H.L. Luong, P.D. Tung, K.D. Pham, P.T. Dang, D.D. Vo, Superlattices Microstruct. 125 (2019) 205.
[9] C.V. Nguyen, N.N. Hieu, N.A. Poklonski, V.V. Ilyasov, L. Dinh, T.C. Phong, L.V. Tung, H.V. Phuc, Phys. Rev. B 96 (2017) 125411.
[10] N.D. Hien, C.V. Nguyen, N.N. Hieu, S.S. Kubakaddi, C.A. Duque, M.E. Mora-Ramos, L. Dinh, T.N. Bich, H.V. Phuc, Phys. Rev. B 101 (2020) 045424.
[11] C.V. Nguyen, N. Hieu, C.A. Duque, D. Khoa, N. Hieu, L. Tung, H. Phuc, J. Appl. Phys. 121 (2017) 045107.
[12] T.V. Vu, H.D. Tong, T.K. Nguyen, C.V. Nguyen, A.A. Lavrentyev, O.Y. Khyzhun, B.V. Gabrelian, H.L. Luong, K.D. Pham, P.T. Dang, D.D. Vo, Chem. Phys. 521 (2019) 5.
[13] H. Şahin, S. Cahangirov, M. Topsakal, E. Bekaroglu, E. Aktürk, R.T. Senger, S. Ciraci, Phys. Rev. B 80 (2009) 155453.
[14] M.H. Crawford, IEEE J. Sel. Top. Quantum Electron. 15 (2009) 1028.
[15] D.F. Feezell, J.S. Speck, S.P. DenBaars, S. Nakamura, J. Display Tech. 9 (2013) 190.
[16] Y. Ota, Solid State Commun. 270 (2018) 147.
[17] X. Liu, C.-K. Tan, Semicond. Sci. Technol. 35 (2020) 025023.
[18] X. Sun, Q. Yang, R. Meng, C. Tan, Q. Liang, J. Jiang, H. Ye, X. Chen, Appl. Surf. Sci. 404 (2017) 291.
[19] D. Liang, R. Quhe, Y. Chen, L. Wu, Q. Wang, P. Guan, S. Wang, P. Lu, RSC Adv. 7 (2017) 42455.
[20] G. Koblmüller, C.S. Gallinat, S. Bernardis, J.S. Speck, G.D. Chern, E.D. Readinger, H. Shen, M. Wraback, Appl. Phys. Lett. 89 (2020) 071902.
[21] X.L. Zhu, L.W. Guo, M.Z. Peng, B.H. Ge, J. Zhang, G.J. Ding, H.Q. Jia, H. Chen, J.M. Zhou, J. Cryst. Growth 310 (2008) 3726.
[22] K. Sasamoto, K.-i. Sugita, A. Hashimoto, A. Yamamoto, J. Cryst. Growth 314 (2011) 62.
[23] J. Jalilian, M. Naseri, S. Safari, M. Zarei, Physica E 83 (2016) 372.
[24] M. Farzan, S. Elahi, M. Abolhassani, H. Salehi, Superlattices Microstruct. 105 (2017) 99.
[25] Q. Peng, X. Sun, H. Wang, Y. Yang, X. Wen, C. Huang, S. Liu, S. De, Appl. Mater. Today 7 (2017) 169.
[26] K.D. Pham, C.V. Nguyen, H.V. Phuc, T.V. Vu, N.V. Hieu, B.D. Hoi, L.C. Nhan, V.Q. Nha, N.N. Hieu, Superlattices Microstruct. 120 (2018) 501.
[27] C.V. Nguyen, N.N. Hieu, V.V. Ilyasov, J. Electron. Mater. 45 (2016) 4038.
[28] N.N. Hieu, H.V. Phuc, V.V. Ilyasov, N.D. Chien, N.A. Poklonski, N.V. Hieu, C.V. Nguyen, J. Appl. Phys. 122 (2017) 104301.
[29] D.D. Vo, T.V. Vu, N.V. Hieu, N.N. Hieu, H.V. Phuc, N.T.T. Binh, L.T.T. Phuong, M. Idrees, B. Amin, C.V. Nguyen, Phys. Chem. Chem. Phys. 21 (2019) 25849.
[30] K.D. Pham, N.N. Hieu, H.V. Phuc, I.A. Fedorov, C.A. Duque, B. Amin, C.V. Nguyen, Appl. Phys. Lett. 113 (2018) 171605.
[31] P.T.T. Le, N.N. Hieu, L.M. Bui, H.V. Phuc, B.D. Hoi, B. Amin, C.V. Nguyen, Phys. Chem. Chem. Phys. 20 (2018) 27856.
[32] H.V. Phuc, N.N. Hieu, B.D. Hoi, C.V. Nguyen, Phys. Chem. Chem. Phys. 20 (2018) 17899.
[33] R. Ruoff, Nat. Nanotechnol. 3 (2008) 10.
[34] T.V. Vu, N.T.T. Anh, D.P. Tran, D. Hoat, N.T. Binh, H.D. Tong, B.D. Hoi, C.V. Nguyen, H.V. Phuc, N.N. Hieu, Superlattices Microstruct. 137 (2020) 106359.
[35] R. Grassi, T. Low, M. Lundstrom, Nano Lett. 11 (2011) 4574.
[36] B.D. Hoi, L.T.T. Phuong, V.T. Lam, D.Q. Khoa, T. Tien, N.T.T. Binh, H.V. Phuc, N.N. Hieu, C.V. Nguyen, RSC Adv. 9 (2019) 41569.
[37] J.M. Zavada, R.G. Wilson, C.R. Abernathy, S.J. Pearton, Appl. Phys. Lett. 64 (1994) 2724.
[38] S.P. Fu, T.J. Lin, W.S. Su, C.Y. Shieh, Y.F. Chen, C.A. Chang, N.C. Chen, P.H. Chang, J. Appl. Phys. 99 (2006) 126102.
[39] P. Giannozzi, S. Baroni, N. Bonini, M. Calandra, R. Car, C. Cavazzoni, D. Ceresoli, G.L. Chiarotti, M. Cococcioni, I. Dabo, A.D. Corso, S. de Gironcoli, S. Fabris, G. Fratesi, R. Gebauer, U. Gerstmann, C. Gougoussis, A. Kokalj, M. Lazzeri, L. Martin-Samos, N. Marzari, F. Mauri, R. Mazzarello, S. Paolini, A. Pasquarello, L. Paulatto, C. Sbraccia, S. Scandolo, G. Sclauzero, A.P. Seitsonen, A. Smogunov, P. Umari, R.M. Wentzcovitch, J. Phys.: Condens. Matter 21 (2009) 395502.
[40] J.P. Perdew, K. Burke, M. Ernzerhof, Phys. Rev. Lett. 77 (1996) 3865.
[41] J.P. Perdew, K. Burke, M. Ernzerhof, Phys. Rev. Lett. 78 (1997) 1396.
[42] A.H. MacDonald, W.E. Picket, D.D. Koelling, J. Phys. C: Solid State Phys. 13 (1980) 2675.
[43] D.R. Hamann, M. Schlüter, C. Chiang, Phys. Rev. Lett. 43 (1979) 1494.
[44] J.P. Perdew, M. Levy, Phys. Rev. Lett. 51 (1983) 1884.
[45] J. Heyd, G.E. Scuseria, M. Ernzerhof, J. Chem. Phys. 118 (2003) 8207.
[46] H.L. Zhuang, A.K. Singh, R.G. Hennig, Phys. Rev. B 87 (2013) 165415.
[47] L. Hedin, Phys. Rev. 139 (1965) A796.
[48] R.S. Mulliken, J. Chem. Phys. 23 (1955) 1833.
[49] A. Delin, P. Ravindran, O. Eriksson, J. Wills, Int. J. Quantum Chem. 69 (1998) 349.
[50] S.Z. Karazhanov, P. Ravindran, A. Kjekshus, H. Fjellvag, B.G. Svensson, Phys. Rev. B 75 (2007) 155104.
[51] P. Ravindran, A. Delin, B. Johansson, O. Eriksson, J.M. Wills, Phys. Rev. B 59 (1999) 1776.